applied optics

Design of a compact device to generate and test beams with orbital angular momentum in the EUV

D. O. Pabon, S. A. Ledesma,* G. F. Quinteiro, and M. G. Capeluto

Departamento de Física, Facultad de Ciencias Exactas y Naturales, Universidad de Buenos Aires and IFIBA, CONICET, Cuidad Universitaria, Buenos Aires 1428, Argentina
**Corresponding author: ledesma@df.uba.ar*

Received 16 June 2017; revised 5 September 2017; accepted 5 September 2017; posted 7 September 2017 (Doc. ID 298013); published 4 October 2017

We present a compact design to generate and test optical-vortex beams with possible applications in the extreme ultraviolet (EUV) region of the electromagnetic spectrum. The device consists of a diffractive mask where both the beam with orbital angular momentum and the reference wavefront to test its phase are generated. In order to show that the proposal would work in the EUV, simulations and proof-of-principle experiments were performed, using typical parameters for EUV holography scaled to visible wavelengths. As the simplest case, we consider the well-known Laguerre–Gaussian (LG)-like beams, which have a single vortex in the propagation axis. To further test the versatility of the device, we consider Mathieu beams, more complex structured beams that may contain several vortices. In the experiment, a spatial light modulator was used to display the mask. As examples, we show the results for a LG-like beam with topological charge $\ell = 1$ and Mathieu beams with topological charge $\ell = 2$ and ellipticity $q = 2$. These results show the potential of the device to generate a variety of beam shapes at EUV wavelengths.

OCIS codes: (140.7240) UV, EUV, and X-ray lasers; (050.4865) Optical vortices; (090.1760) Computer holography; (090.1970) Diffractive optics; (140.3300) Laser beam shaping; (040.7480) X-rays, soft x-rays, extreme ultraviolet (EUV).

https://doi.org/10.1364/AO.56.008048

1. INTRODUCTION

Extreme ultraviolet (EUV) compact light sources covering the range of wavelengths from 10 nm to 50 nm, have been proven to be successful not only for basic research but also for a wide variety of applications. Some examples are the characterization and processing of materials [1–3]; techniques for high-resolution metrology [4,5]; studies in atomic physics, photochemistry, and photophysics [6,7]; biological imaging [8–12]; the diagnosis of very-high-density plasmas [13–15]; the study of nonlinear phenomena [16,17]; and even integrated circuit nanolithography [18].

Since the invention of the laser, all different applications that use laser beams have specific demands on beam shape, including intensity or phase distribution, polarization, momentum, and propagation properties. It has been shown that a sharper focus can be obtained for a radially polarized beam [19] with improvement in laser cutting [20]. Nano needle fabrication by ablation was also shown to be improved by using vortex beams instead of a regular doughnut-shaped beam [21], with the extra advantage of reducing the debris.

Although beam shaping is routine at visible wavelengths, it is not as well established at the EUV region of the spectrum, as its implementation is more complex due to the lack of refractive optics. This deficiency, produced by the high absorption in any material makes EUV experiments to exploit the use of reflective optics at grazing incidence or diffractive optics (binary elements, Fresnel zone plates, or gratings). One example of beam shaping, although indirect, is the circularly polarized harmonics [22]. Also, spiral zone plates have been used for phase-sensitive microscopy using synchrotron radiation [23]. Nevertheless, the implementation of beam-shaping strategies with EUV lasers could have high impact in applications such as imaging, lithography, and ablation, where the combination of beam shaping with a short wavelength could lead to improving spatial resolution.

Among the large variety of beams that are nowadays known, optical-vortex (OV) beams have recovered great importance for their wide range of applications as optical traps [24], quantum simulation algorithms with classical light [25], spectroscopy [26] and to study atmospheric turbulences [27]. Despite these, some of the applications mentioned above could benefit from using both short wavelengths and a vortex beam. An EUV OV beam, could reduce significantly the size of micro-machined elements [21]. It can also be important in plasma diagnosis, where EUV wavelengths have the advantage that they can penetrate plasmas with electron densities approaching

solid density [13,14], or to implement an EUV vortex-beam plasma diagnosis technique that could be used for laser Doppler spectroscopy [28].

A vortex in an optical field is a singularity where the phase is not defined. This singularity is maintained as the field propagates, and it is seen as a point singularity in the transverse cross section of the beam. The well-known Laguerre–Gaussian (LG) beams are solutions of the paraxial wave equation in cylindrical coordinates with a single phase singularity, around which the phase changes as an integer multiple ℓ of 2π, where ℓ is also known as the topological charge. A vortex beam with topological charge ℓ carries orbital angular momentum $\ell\hbar$, with $\hbar$ the reduced Planck constant. Mathieu beams satisfy the Helmholtz equation in elliptical coordinates. They exhibit multiple vortices, depending on its ellipticity. In contrast to LG, Mathieu beams are non-diffractive, which makes them very important in applications such as lithography and imaging [29–31].

The techniques to generate beams with orbital angular momentum (OAM) are relatively easy to implement at visible wavelengths with the use of phase or amplitude masks, including spatial light modulators (SLMs). Since the pioneer papers in the 1990s, several designs and applications have been reported; see, e.g., [32]. Among the techniques used to generate vortices, we can cite two of the most frequently used: one of them is to modify directly the wavefront (in amplitude and phase) and the other is to generate a hologram and obtain the vortex beam in its reconstruction. Regarding the first way of generation, as it was mentioned before, due to the great absorption of most materials at EUV wavelengths, it is not possible to fabricate refractive optics. Some proposals of x rays have been developed employing phase plates fabricated with sophisticated techniques such as ablation [33,34] and where an independent setup is used to study the phase interferometrically [35]. The second technique has the advantage that EUV holograms can be represented in binary media without a significant loss of information. These kinds of binary elements are feasible to fabricate, placing them as attractive candidates for generation of OV in the EUV.

In order to test the beam's vorticity, an interferometric setup is required. In general, this is accomplished by means of interferometers, e.g., Michelson or Mach–Zehnder architectures.

In this work, we present a compact device to generate and test beams with OAM for its applications in the EUV region of the spectrum. The device consists of a binary mask that contains the necessary information to generate the OV itself and a reference wavefront to test its phase. Our proposal avoids the use of extra optical elements and simplifies the processes of testing as well as of alignment of amplitude division interferometers in the EUV. We demonstrate the device performance and versatility by a combination of numerical analyses and proof-of-principle experiments at visible wavelengths using an SLM. We first consider the generation and measurement of the simple—but very practical—case of LG-like beams, and then the more complex case of Mathieu beams. Our results strongly suggest that the device can be easily used to produce and measure any beam shape generated by a binary Fourier hologram. In Section 2, we describe the computer-generated holograms (CGHs) used to produce the vortex beams, and in Section 3, we show the mask to generate and test the vortex beams. Numerical simulations are presented in Section 4, and the experimental results are shown in Section 5.

2. CGH FOR GENERATING ORBITAL ANGULAR MOMENTUM BEAMS

A. LG-Like Vortices

The spatial dependence of a first-order LG beam that propagates in the z direction can be expressed as

$$E_{\mathrm{LG}}(r,\theta,z) = A_0^{\ell}(r,z)e^{i\ell\theta}e^{ik_z z}, \tag{1}$$

where (r,θ,z) are cylindrical coordinates related to the Cartesian system (x,y,z) by $r=\sqrt{(x^2+y^2)}$, $\theta=\tan^{-1}(y/x)$, and $z=z$, ℓ is an integer number, and k_z is the wavenumber. The factor $e^{i\ell\theta}$ in equation (1) gives the characteristic helicity to the wavefront, with a topological charge ℓ. The modulus of ℓ indicates the number of intertwined helical surfaces and the sign its handedness. $A_0^{\ell}(r,z)$ is the amplitude distribution given by [36]

$$A_0^{\ell}(r,z) = \left(\frac{2}{\pi!|\ell|!\omega^2(z)}\right)^{1/2}\left(\frac{\sqrt{2}r}{\omega(z)}\right)^{|\ell|} e^{-\frac{r^2}{\omega^2(z)}} e^{-\frac{ikr^2}{|2R(z)|}} e^{-i\varphi(z)}, \tag{2}$$

where $R(z)$, $\omega(z)$, and $\varphi(z)$ are the radius of curvature, the evolving beam width, and the Gouy phase of the beam, respectively.

Usually LG-like vortices are created by using fork holograms, which are obtained from the interference of a spiral phase and a plane wave. Although these kinds of holograms do not produce the exact LG radial profile [Eq. (2)]—and for this reason we call them here LG-like beams—the holograms convey the correct helicity to the beam [37,38]. These kinds of beams are commonly known as Kummer beams [38]. The fork Fourier holograms are obtained from the interference of a plane wave and a vortex given by $\psi_1(\theta,z) = A_1 e^{i\ell\theta}e^{ik_z z}$, with A_1 a constant amplitude. A plane wave of amplitude A_2 that propagates in the xz plane can be written as $\psi_2(x,z) = A_2 e^{ik_x x}e^{ik_z z}$, where k_x (k_z) is the component of the wave vector in the direction $x(z)$. The normalized intensity of the interference pattern is given by $I = |A_1^2 + A_2^2 + 2A_1A_2\cos(\ell\theta - k_x x)|/(A_1^2+A_2^2)$. Given that both the LG beam and its Fourier transform have the same spiral phase, the fork hologram can be thought as an object-phase hologram or as a Fourier-phase hologram. It should be noted that the far-field condition is easily obtained at a shorter wavelength such as EUV, and then it is adequate to consider Fourier holograms for EUV beam shaping. In Fig. 1(a), we show the spiral phases corresponding to OAM beams (and the phase of their Fourier transforms) with $\ell = 1, 2, 3$. The phases (modulus 2π) are shown in grayscale where black represents 0, and white represents 2π. The phase at the center of the wavefront is not defined, and the line indicates the change in 2π. In Fig. 1(b), we show the binarized fork holograms where the typical bifurcations at the central groove are clearly seen.

B. Mathieu Vortices

Mathieu beams are solutions of the Helmholtz equation in elliptic cylindrical coordinates (ξ,η,z), that are related to the Cartesian coordinates by $x = h\cos(\eta)\cosh(\xi)$, $y = h\sin(\eta)\sinh(\xi)$, and $z=z$, where $\xi\in[0,\infty]$, $\eta\in[0,2\pi]$,

and $z \in [-\infty, \infty]$. In these coordinates, a constant value of ξ defines ellipses, and a constant value of η defines hyperbolas. The parameter h is the position of the foci of these surfaces, located at $-h$ and h in the x axis. The elliticity of the beam is defined as $q = k_t h^2/4$, where k_t is the transverse component of the wave vector. Both wave vector components, transversal (k_t) and longitudinal (k_z), are related to the modulus of the wave vector by $k^2 = k_t^2 + k_z^2$. The electric field [39] that describes a Mathieu beam is given by

$$E_\ell(\eta, \xi, z; q) = [A_\ell(q) Je_\ell(\xi; q) ce_\ell(\eta; q) + iB_\ell(q) Jo_\ell(\xi; q) se_\ell(\eta; q)] \exp(ik_z z), \quad (3)$$

where $Je_\ell(\xi; q)$ and $Jo_\ell(\xi; q)$ are the radial even and odd solutions, respectively; $ce_\ell(\eta; q)$ and $se_\ell(\eta; q)$ are the angular even and odd solutions of Mathieu's equation, respectively; and similar to the LG-like vortex beam, ℓ is the topological charge. As it has been proved by Chávez-Cerda *et al.* [39], in the case of $\ell \geq 2$ and $q \leq \ell^2/2 - 1$, the evaluation of the coefficients $A_\ell(q)$ and $B_\ell(q)$ yields $A_\ell(q) \approx B_\ell(q)$. Considering Eq. (3) and assuming $z = 0$, the amplitude $|E_\ell(\eta, \xi, z = 0; q)|$ and the phase $\varphi_\ell(\eta, \xi; q)$ of the electromagnetic field can be written as follows:

$$|E_\ell(\eta, \xi, z = 0; q)| = A_\ell(q)\{[Je_\ell(\xi; q) ce_\ell(\eta; q)]^2 + [Jo_\ell(\xi; q) se_\ell(\eta; q)]^2\}^{\frac{1}{2}}$$

$$\varphi_\ell(\eta, \xi; q) = \arctan[Jo_\ell(\xi; q) se_\ell(\eta; q)/Je_\ell(\xi; q) ce_\ell(\eta; q)]. \quad (4)$$

The Fourier hologram is computed from the interference between the electromagnetic field distribution at $z = 0$ and a plane wave.

As an example, in Fig. 2, we show the Mathieu beam for $\ell = 2$ and $q = 2$. Figure 2(a) shows the amplitude and phase distribution where, in contrast to the case of LG-like beams (Fig. 1), a set of vortices is clearly seen in the magnified view of the phase distribution. In Fig. 2(b), the fast Fourier transform is represented. The phase (modulus 2π) is shown in grayscale, where black represents 0, and white represents 2π.

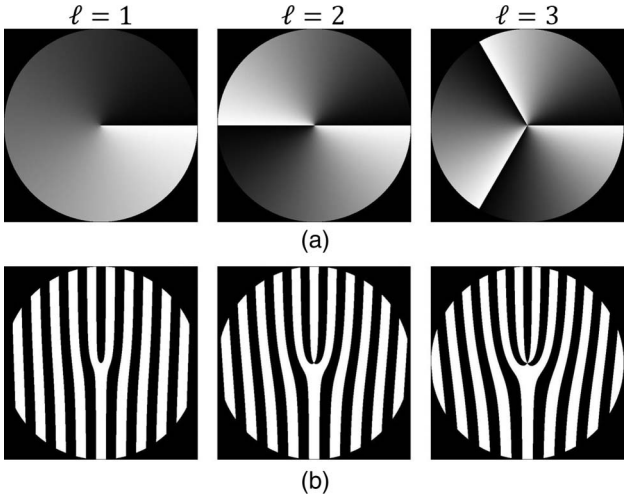

Fig. 1. (a) Phase mask and (b) binary fork holograms for a topological charge value $\ell = 1, 2, 3$.

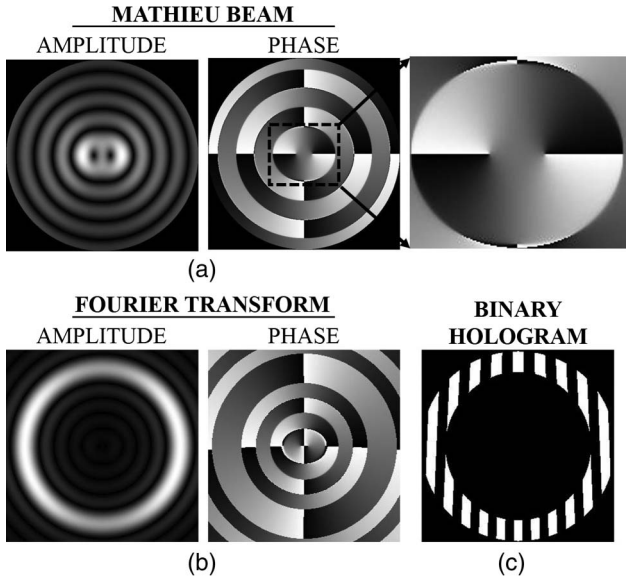

Fig. 2. (a) Representation of the amplitude and phase for a Mathieu beam with topological charge $\ell = 2$ and $q = 2$. (b) Fourier transform of (a). (c) Binarized Fourier hologram.

For the case of the Fourier spectrum, the amplitude is mainly distributed over an annular ring, as can be observed in Fig. 2(b). The binarized version of the Fourier hologram is shown in Fig. 2(c).

3. DEVICE DESCRIPTION AND NUMERICAL SIMULATIONS

To generate and test with a single setup a beam carrying OAM, we propose a device containing a mask that has in the same plane a binary Fourier hologram of a vortex beam and a laterally displaced pinhole. This would be very useful for testing the correct generation of the beams, since, e.g., a failure in mask construction or misalignment could cause deviation from the desired beam. Figure 3 presents the geometrical design of the mask, which consists of a pinhole and a CGH laterally displaced. The vortex beam is generated at the far field plane of the mask, and it would be observed by blocking the pinhole. To characterize the beam phase, it is necessary to produce an interference pattern, which can be accomplished by unblocking the pinhole. Using this mask, the experiment can be done by using only a Fresnel zone plate as an extra optics, minimizing the number of elements required in the experiment and maximizing its throughput. The design of the device is based on the

Fig. 3. Schematic of the mask composed by a pinhole and a binarized amplitude hologram.

concept of point diffraction interferometry, and a similar idea was used by Monserud *et al.* [40] to study the oscillatory dynamics of cantilevers, through EUV holography.

In practice, the throughput ratio between the two parts of the mask (pinhole and hologram) should be considered to obtain good visibility on the interference pattern. In order to get more light through the pinhole, Monserud *et al.* [40] used a binary zone plate as a beam splitter to generate an intense reference beam and illuminate the hologram. The laser beam is focused on the pinhole using the first-order focus of the binary zone plate. This allows us to have high intensity through the pinhole and filter the higher diffraction orders at the zone-plate. The central opening in the zone plate allowed the incident beam to directly illuminate the object with an almost plane wavefront. The same scheme of illumination could be used in this setup to obtain good visibility.

Figure 4(a) shows the mask to generate the LG-like vortex beam with topological charge $\ell = 1$. In this case, the classical doughnut beam profile would be observed in the far field by covering the pinhole. In Fig. 4(b), numerical results of the reconstruction of the binary hologram shown in Fig. 4(a) are plotted. At the center of orders +1 and −1, a zero-intensity point is visible, indicating the possible existence of a vortex in the propagation axis. However, to completely characterize the beam wavefront, it is necessary to determine its phase, which is done by interfering the vortex with a reference beam. In our proposal, the reference wavefront would be produced when light is diffracted at the pinhole. The bifurcation in the interference pattern in Fig. 4(c) unambiguously indicates the existence of a phase singularity at the propagation axis. The number of bifurcations is related to the topological charge of the beam; in this case, $\ell = 1$ yields one bifurcation.

Figure 5(a) shows the mask for the reconstruction of Mathieu beams, in the case of $\ell = 2$ and $q = 2$. In Fig. 5(b), the diffracted orders are shown when the pinhole is blocked, and in Fig. 5(c), the interference pattern obtained unblocking the pinhole can be observed. The mask reproduces the amplitude distribution, as seen in Fig. 2(a). A direct comparison with the phase distribution shown in Fig. 2(a) is not possible, since Fig. 5(c) presents the interference between the Mathieu beam and the output of the device pinhole. However, fork-like bifurcations are clearly distinguishable, which, in connection to the well-known result of Fig. 1(b) for LG beams, indicates the existence of singularities in the output beam from the Mathieu reconstruction mask. Moreover, we will see in Section 4 that the simulations are in good agreement with the experiment.

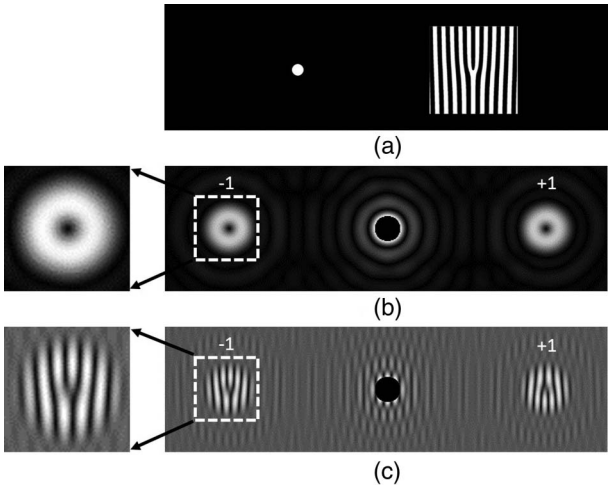

Fig. 4. (a) Schematic of the mask composed by a pinhole and a binarized amplitude hologram, (b) simulated intensity pattern in the far field with a blocked pinhole, and (c) simulated intensity in the far field revealing the interference pattern by unblocking the pinhole.

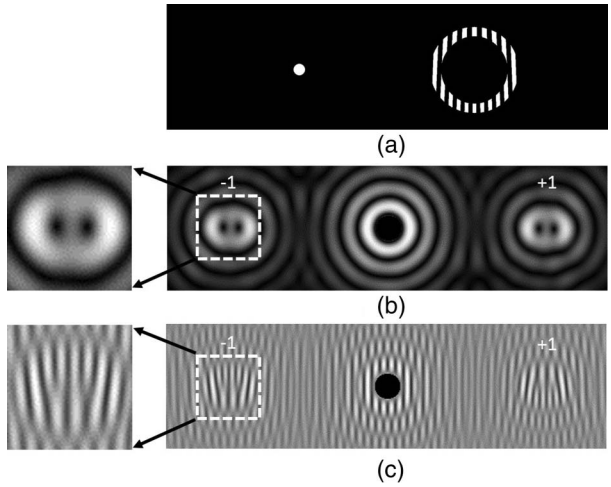

Fig. 5. (a) Mask to generate the Mathieu beam, (b) far-field simulated diffraction pattern without blocking the pinhole, and (c) far-field simulated diffraction pattern by unblocking the pinhole.

4. PROOF-OF-PRINCIPLE EXPERIMENT AT VISIBLE WAVELENGTHS

Due to the great complexity involved in making experiments at EUV (high absorption and only vacuum propagation), it is a usual practice to scale experiments to visible wavelengths to experimentally proof their performance. We designed the device for visible wavelengths, using the scaled dimensions that would be used in EUV, and we used a SLM to display the mask. As it was mentioned before, the light throughput from the pinhole and hologram should be about the same to obtain good visibility on the interference pattern. Following the idea used in Monserud *et al.* [40] where a Fresnel zone plate is used to simultaneously illuminate the pinhole and the object whose hologram will be produced, and taking the advantage of SLMs to display different objects simultaneously, we used a Fresnel zone plate in place of the pinhole. Choosing an adequate focal distance, the zone plate produces in the far field the same effect that the pinhole.

The experimental verification of the method at visible range was made by using the experimental setup shown in Fig. 6. A He–Ne laser is spatial filtered and expanded using a microscopic objective (O), a pinhole (PH), and a lens (L_1). This produces a plane wave that fully illuminates the SLM screen. A beam splitter was used in such a way that the laser impinges

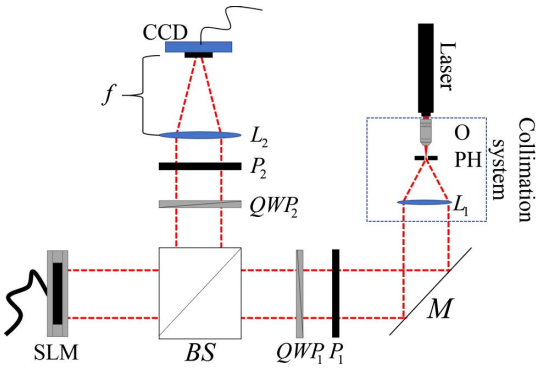

Fig. 6. Experimental setup: (O) microscope objective, (PH) pinhole. (L_1). (BS) beam splitter 50:50. (SLM) spatial light modulator. (L_2) lens with focal distance $f = 11.5$ cm. (CCD) camera of visualization and acquisition results. (M) mirror. (P_1, P_2) linear polarizers. (QWP_1, QWP_2) quarter waveplates.

normal to the SLM, and the reflected light is directed to the detection system.

The SLM (LC-R 2500 Holoeye) of 1024×768 pixels was placed between linear polarizers (P_1, P_2) and quarter waveplates (QWP_1, QWP_2) in a configuration that provides phase-only modulation, which leads to higher efficiency in the diffracted orders [41]. The focal distance of the lens L_2 is equal to the focal distance of the Fresnel zone plate displayed in the SLM ($f = 11.5$ cm). A monochromatic charge-coupled device (CCD) (1024×768 pixels) was used as a register medium.

The size of the binarized fork holograms and the Fresnel lens were 60×60 pixels (each pixel of the SLM has an area of 19×19 μm^2), the period of the fork hologram was 6 pixels, and the focal distance of the Fresnel zone plate was of $f = 11.5$ cm. These parameters were calculated by scaling up experimental parameters from Monserud *et al.* [40], where a 46.7 nm laser is used to illuminate a mask with 1 μm resolution and total lateral size of 150 μm. Figure 7 shows the results on generation and detection of an OAM LG-like beam. On one hand, by blocking the Fresnel zone plate, we observed the classical doughnut-shaped spatial intensity distribution of one of the diffracted orders at the fork hologram [Fig. 7(a)]. On the other hand, when the Fresnel zone plate is unblocked, the interference pattern between the reference plane wave and the same diffracted order is observed [Fig. 7(b)]. The typical bifurcation at the interference pattern supports that the tested beams in Fig. 7(a) are beams with OAM with topological charge $\ell = 1$. Figures 7(c) and 7(d) show a Mathieu beam obtained from the first order diffracted by the mask shown in Fig. 5(a). Figure 7(c) shows the beam with the pinhole blocked and Fig. 7(d) shows the interference pattern used to reveal the phase. The phase distribution exhibits two important features. First, two fork-like displaced bifurcations inside the main ellipse can be observed, which indicates the existence of the field's singularities located at different positions as opposed to what happens for a LG beam having a single singularity at $r = 0$ [see Fig. 1(b)]. Second, clear dislocations in fringes between neighbor ellipses are seen. The phase features are also observed in the numerical simulation shown in Fig. 5(c). Overall,

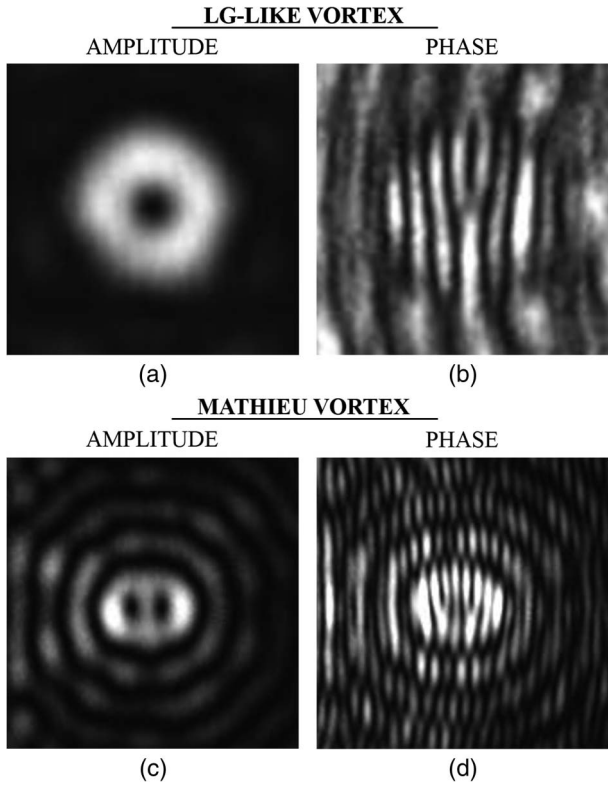

Fig. 7. Images of the intensity distribution registered by the CCD camera for the LG-like beam and Mathieu beam. Far-field diffraction pattern for the first diffracted order (a)–(c) without blocking the Fresnel zone plate and (b)–(d) unblocking it.

experimental and numerical simulations are in good agreement and demonstrate that the device can produce and test the expected beam.

5. CONCLUSIONS

In this work, we show a design of a compact device to generate and characterize beams with OAM with applications in the EUV. The device consists of a binary mask that contains a hologram and a pinhole. The hologram produces the desired OAM beam while the pinhole a reference beam, which allows testing the phase distribution. Because binary masks and reflective optics are the only possible choices at the EUV wavelength, the hologram must be binarized. We study the performance of the device by a combination of numerical simulations and proof-of-principle experiments by scaling up to visible wavelengths and using a Fresnel lens instead of the pinhole. In the experiment, we used a SLM to represent both the Fresnel lens and the hologram.

Two kinds of OVs were produced and characterized. First, we considered a LG-like beam with topological charge $\ell = 1$, due to its simplicity and extensive use. Then, we considered the more complex case of the Mathieu beam with topological $\ell = 2$ and ellipticity $q = 2$. In both cases, the far-field intensity distribution and the interference pattern behave as expected. The intensity distribution has a doughnut or centered ellipses shape that corresponds to the typical intensity

distribution of a LG beam or a Mathieu beam, respectively. For the case of LG-like beams, the interference pattern shows the characteristic bifurcation in the center, while the Mathieu beam exhibits few displaced dislocations, each one corresponding to a vortex.

The device shows the potential to generate and test arbitrary beam shapes carrying OAM, expanding the possible applications in the EUV.

Funding. Agencia Nacional de Promoción de Ciencia y Técnica (ANPCyT) (2013-592, 2014-2432, 2014-3537); Consejo Nacional de Investigaciones Científicas y Técnicas (CONICET) (PIP2015-2017 112201 501004 75CO).

Acknowledgment. We thank Prof. Mario Marconi for the useful discussions.

REFERENCES

1. H. Fiedorowicz, A. Bartnik, P. W. Wachulak, R. Jarocki, J. Kostecki, M. Szczurek, I. U. Ahad, T. Fok, A. Szczurek, and Ł. Węgrzyński, "Application of laser plasma sources of soft x-rays and extreme ultraviolet (EUV) in imaging, processing materials and photoionization studies," in *X-Ray Lasers*, Springer Proceedings in Physics (Springer International Publishing, 2014), Vol. **169**, pp. 369–377.
2. V. Aslanyan, I. Kuznetsov, H. Bravo, M. R. Woolston, A. K. Rossall, C. S. Menoni, J. J. Rocca, and G. J. Tallents, "Ablation and transmission of thin solid targets irradiated by intense extreme ultraviolet laser radiation," APL Photon. **1**, 066101 (2016).
3. P. Daukantas, S. Michaud, I. Ostri, and S. Wills, "Research and industry news," Opt. Photon. News **28**(2), 8–13 (2017).
4. R. Miyakawa and P. Naulleau, "Extending shearing interferometry to high-NA for EUV optical testing," Proc. SPIE **9422**, 94221J (2015).
5. M. G. Capeluto, M. C. Marconi, and C. C. Iemmi, "Design of a phase-shifting interferometer in the extreme ultraviolet for high-precision metrology," Appl. Opt. **53**, 1274–1283 (2014).
6. E. T. Kennedy, J. T. Costello, J. P. Mosnier, and P. van Kampen, "VUV/EUV ionising radiation and atoms and ions: dual laser plasma investigations," Radiat. Phys. Chem. **70**, 291–321 (2004).
7. Y. Hatano, "Spectroscopy and dynamics of molecular superexcited states. Aspects of primary processes of radiation chemistry," Radiat. Phys. Chem. **67**, 187–198 (2003).
8. I. Kuznetsov, J. Filevich, F. Dong, M. Woolston, W. Chao, E. H. Anderson, E. R. Bernstein, D. C. Crick, J. J. Rocca, and C. S. Menoni, "Three-dimensional nanoscale molecular imaging by extreme ultraviolet laser ablation mass spectrometry," Nat. Commun. **6**, 6944 (2015).
9. D. T. Attwood, E. Anderson, G. Denbeaux, K. Goldberg, P. Naulleau, and G. Schneider, "Soft x-ray microscopy and EUV lithography: an update on imaging at 20–40 nm spatial resolution," AIP Conf. Proc. **641**, 461–468 (2002).
10. J. Miao, T. Ishikawa, I. K. Robinson, and M. M. Murnane, "Beyond crystallography: diffractive imaging using coherent x-ray light sources," Science **348**, 530–535 (2015).
11. D. Shapiro, P. Thibault, T. Beetz, V. Elser, M. Howells, C. Jacobsen, J. Kirz, E. Lima, H. Miao, A. M. Neiman, and D. Sayre, "Biological imaging by soft x-ray diffraction microscopy," Proc. Natl. Acad. Sci. USA **102**, 15343–15346 (2005).
12. H. Jiang, C. Song, C. Chen, R. Xu, K. S. Raines, B. P. Fahimian, C.-H. Lu, T.-K. Lee, A. Nakashima, J. Urano, T. Ishikawa, F. Tamanoi, and J. Miao, "Quantitative 3D imaging of whole, unstained cells by using X-ray diffraction microscopy," Proc. Natl. Acad. Sci. USA **107**, 11234–11239 (2010).
13. J. Filevich, K. Kanizay, M. C. Marconi, J. L. Chilla, and J. J. Rocca, "Dense plasma diagnostics with an amplitude-division soft-x-ray laser interferometer based on diffraction gratings," Opt. Lett. **25**, 356–358 (2000).
14. J. Filevich, J. J. Rocca, M. C. Marconi, S. J. Moon, J. Nilsen, J. H. Scofield, J. Dunn, R. F. Smith, R. Keenan, J. R. Hunter, and V. N. Shlyaptsev, "Observation of a multiply ionized plasma with index of refraction greater than one," Phys. Rev. Lett. **94**, 035005 (2005).
15. M. A. Purvis, J. Grava, J. Filevich, M. C. Marconi, J. Dunn, S. J. Moon, V. N. Shlyaptsev, E. Jankowska, and J. J. Rocca, "Soft X-ray laser interferometry of colliding laser-created plasmas in semicylindrical cavities," IEEE Trans. Plasma Sci. **36**, 1134–1135 (2008).
16. C. Conti, A. Fratalocchi, G. Ruocco, and F. Sette, "Nonlinear optics in the X-ray regime: nonlinear waves and self-action effects," Opt. Express **16**, 8324–8331 (2008).
17. T. Popmintchev, M. Chen, P. Arpin, M. M. Murnane, and H. C. Kapteyn, "The attosecond nonlinear optics of bright coherent x-ray generation," Nat. Photonics **4**, 822–832 (2010).
18. C. Wagner and N. Harned, "EUV lithography: lithography gets extreme," Nat. Photonics **4**, 24–26 (2010).
19. R. Dorn, S. Quabis, and G. Leuchs, "Sharper focus for a radially polarized light beam," Phys. Rev. Lett. **91**, 233901 (2003).
20. M. Meier, V. Romano, and T. Feurer, "Material processing with pulsed radially and azimuthally polarized laser radiation," Appl. Phys. A **86**, 329–334 (2007).
21. T. Omatsu, K. Chujo, K. Miyamoto, M. Okida, K. Nakamura, N. Aoki, and R. Morita, "Metal microneedle fabrication using twisted light with spin," Opt. Express **18**, 17967–17973 (2010).
22. O. Kfir, P. Grychtol, E. Turgut, R. Knut, D. Zusin, D. Popmintchev, T. Popmintchev, H. Nembach, J. M. Shaw, A. Fleischer, H. Kapteyn, M. Murnane, and O. Cohen, "Generation of bright phase-matched circularly-polarized extreme ultraviolet high harmonics," Nat. Photonics **9**, 99–105 (2015).
23. A. Sakdinawat and Y. Liu, "Soft-x-ray microscopy using spiral zone plates," Opt. Lett. **32**, 2635–2637 (2007).
24. D. B. Ruffner and D. G. Grier, "Optical forces and torques in nonuniform beams of light," Phys. Rev. Lett. **108**, 173602 (2012).
25. B. Perez-Garcia, J. Francis, M. McLaren, R. I. Hernandez-Aranda, A. Forbes, and T. Konrad, "Quantum computation with classical light: the Deutsch algorithm," Phys. Lett. A **379**, 1675–1680 (2015).
26. Y. Toda, K. Shigematsu, K. Yamane, and R. Morita, "Efficient Laguerre-Gaussian mode conversion for orbital angular momentum resolved spectroscopy," Opt. Commun. **308**, 147–151 (2013).
27. V. P. Aksenov, V. V. Dudorov, and V. V. Kolosov, "Properties of vortex beams formed by an array of fiber lasers and their propagation in a turbulent atmosphere," Quantum Electron. **46**, 726–732 (2016).
28. S. Yoshimura, M. Aramaki, N. Ozaw, K. Terasaka, M. Tanaka, K. Nagaoka, and T. Morisaki, "Azimuthal Doppler shift of absorption spectrum in optical vortex laser absorption spectroscopy," in *58th Annual Meeting of the APS Division of Plasma Physics* (2016), Vol. **61**.
29. J. Yin, W. Gao, and Y. Zhu, "Generation of dark hollow beams and their applications," in *Progress in Optics*, E. Wolf, ed. (Elsevier, 2003), Vol. **45**, pp. 196.
30. C. Alpmann, R. Bowman, M. Woerdemann, M. Padgett, and C. Denz, "Mathieu beams as versatile light moulds for 3D micro particle assemblies," Opt. Express **18**, 26084–26091 (2010).
31. C. Lopez-Mariscal, J. C. Gutierrez-Vega, V. Garces-Chavez, and K. Dholakia, "Observation of the angular momentum transfer in the Mie regime using Mathieu beams," Proc. SPIE **5930**, 59301U (2005).
32. A. M. Yao and M. J. Padgett, "Orbital angular momentum: origins, behavior and applications," Adv. Opt. Photon. **3**, 161–204 (2011).
33. A. G. Peele, P. J. McMahon, D. Paterson, C. Q. Tran, A. P. Mancuso, K. A. Nugent, J. P. Hayes, E. Harvey, B. Lai, and I. McNulty, "Observation of an x-ray vortex," Opt. Lett. **27**, 1752–1754 (2002).
34. A. G. Peele, K. A. Nugent, A. P. Mancuso, D. Paterson, I. McNulty, and J. P. Hayes, "X-ray phase vortices: theory and experiment," J. Opt. Soc. Am. A **21**, 1575–1584 (2004).
35. B. Terhalle, A. Langner, B. Päivänranta, V. A. Guzenko, C. David, and Y. Ekinci, "Generation of extreme ultraviolet vortex beams using computer generated holograms," Opt. Lett. **36**, 4143–4145 (2011).
36. D. L. Andrews, *Structured Light and its Applications: An Introduction to Phase-Structured Beams and Nanoscale Optical Forces* (Academic, 2011).

37. N. R. Heckenberg, R. McDuff, C. P. Smith, H. Rubinsztein-Dunlop, and M. J. Wegener, "Laser beams with phase singularities," Opt. Quantum Electron. **24**, S951–S962 (1992).
38. A. Y. Bekshaev and A. I. Karamoch, "Spatial characteristics of vortex light beams produced by diffraction gratings with embedded phase singularity," Opt. Commun. **281**, 1366–1374 (2008).
39. S. Chávez-Cerda, J. C. Gutiérrez-Vega, and G. H. C. New, "Elliptic vortices of electromagnetic wave fields," Opt. Lett. **26**, 1803–1805 (2001).
40. N. C. Monserud, E. B. Malm, P. W. Wachulak, V. Putkaradze, G. Balakrishnan, W. Chao, E. Anderson, D. Carlton, and M. C. Marconi, "Recording oscillations of sub-micron size cantilevers by extreme ultraviolet Fourier transform holography," Opt. Express **22**, 4161–4167 (2014).
41. A. Marquez, C. Iemmi, I. Moreno, J. Davis, J. Campos, and M. Yzuel, "Quantitative predictions of the modulation behavior of twisted nematic liquid crystal displays based on a simple physical model," Opt. Eng. **40**, 2558–2564 (2001).